Zhang *et al. Biochar* (2026) 8:2
https://doi.org/10.1007/s42773-025-00512-9

Biochar

ORIGINAL RESEARCH Open Access

Efficient allelochemical removal from continuous capsicum cultivation using horseradish peroxidase–loaded biochar

Xueyan Zhang[1,2†], Shiyu Lv[1,2†], Tian Yuan[1,2], Kerong Fu[1,2], Pu Yang[1,2], Yanpo Yao[1], Junfeng Liang[1], Tongguo Gao[3] and Feng Wang[1,2*]

Abstract

Secretion and long-term accumulation of phenolic acid allelopathic substances are critical factors decreasing yield in continuous capsicum cropping systems. However, there are limited effective technologies and methods for removing these substances. In this study, biochar (BC) with ultrahigh specific surface area and pore volume was prepared via K_2CO_3 etching, called carbonate-modified biochar (CBC). Then, it was loaded with horseradish peroxidase (HRP) under glutaraldehyde crosslinking conditions to form HRP–CBC. The maximum loading capacity of HRP reached 311.46 U g^{-1}. Under various factors, the degradation efficiency of allelopathic substances such as ferulic acid followed the order HRP–CBC > HRP–BC > HRP, indicating that the combination of alkaline etching and enzyme immobilization enhances ferulic acid degradation. At a HRP–CBC dose of 2 U mL^{-1} and pH 7, the degradation of 20 mg L^{-1} ferulic acid was achieved within 6 h. Furthermore, this method demonstrated excellent degradation performance against multiple phenolic acid compounds responsible for yield reduction in continuous chili pepper cropping systems. HRP–CBC exhibited superior stability, enhanced stress resistance, and broad application potential. The inhibitory effect of ferulic acid on chili seed germination disappeared after degradation by immobilized HRP. Liquid chromatography–mass spectrometry and ecotoxicity analyses confirmed that HRP–CBC degraded ferulic acid into less toxic small organic molecules through a free radical-mediated mechanism. Therefore, a modified biochar immobilized with HRP offers a promising strategy for removing phenolic acid allelopathic substances from continuous cropping systems.

Highlights

- K_2CO_3-etched biochar achieved a maximum horseradish peroxidase loading of 311.46 U g^{-1}.
- Horseradish peroxidase removed/degraded ferulic acid and phenolic acids.
- Modified biochar-immobilized horseradish peroxidase offers a new solution to phenolic autotoxicity.

Keywords Horseradish peroxidase, Biochar, Immobilization, Ferulic acid, Self-toxic substances, Degradation

† Xueyan Zhang and Shiyu Lv have contributed equally to this work.

*Correspondence:
Feng Wang
wangfeng_530@163.com
Full list of author information is available at the end of the article

Graphical Abstract

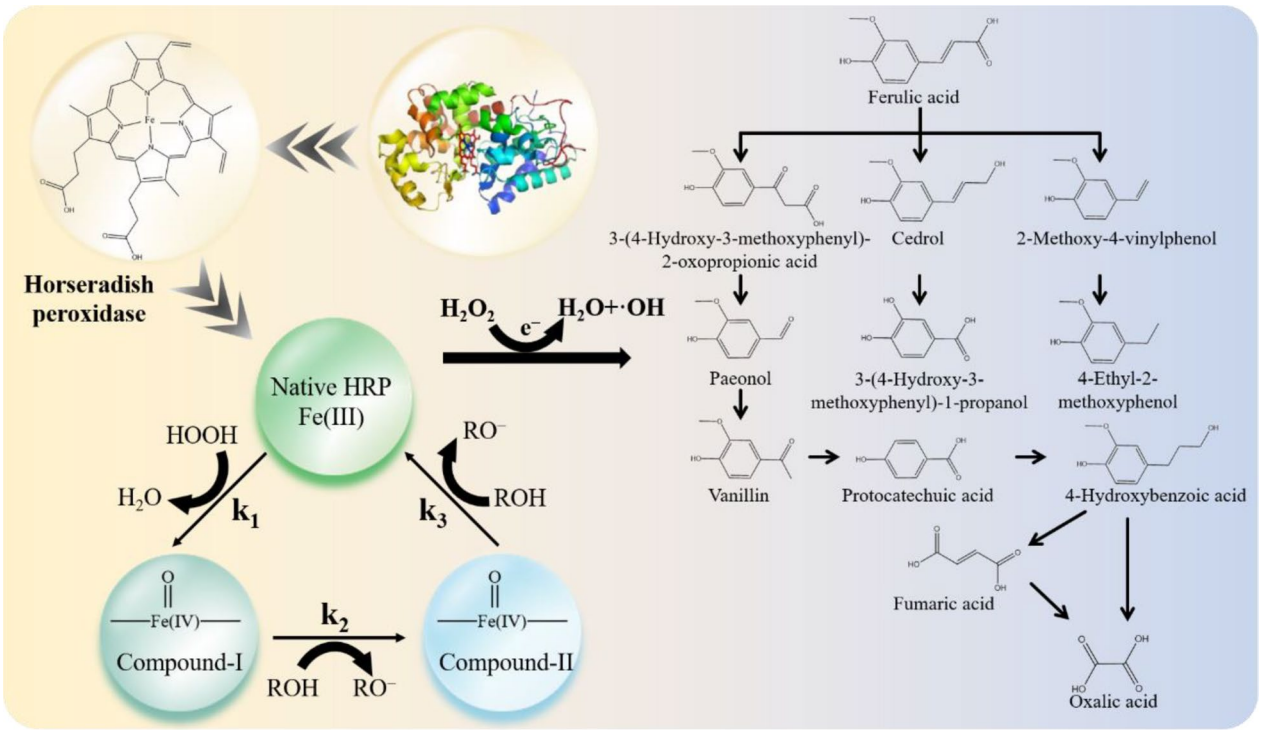

1 Introduction

Capsicum (pepper) is among the most significant global vegetable, possessing relatively high nutritional and economic values. Constraints on arable land availability, coupled with strong market demand, have resulted in widespread use of consecutive cropping practices for pepper. Continuous cultivation for > 20 years can severely inhibit pepper growth and even result in plant death (Chen et al. 2021a, b; Mao et al. 2020). For capsicum, self-toxic substances produced by the root system, such as ferulic acid, p-hydroxybenzoic acid, vanillic acid, cinnamic acid, and coumaric acid, are key obstacles to consecutive cropping (Jia et al. 2024; Wang et al. 2019; Yin et al. 2024). These substances progressively accumulate in soil, inhibiting cell division, suppressing related gene expression, reducing plant hormone levels and activity, and impeding water and nutrient absorption by the root system (Wang et al. 2023). Moreover, among these substances, the concentration of ferulic acid in soil is relatively high, approximately 7.44 μg g^{-1} (Chen et al. 2020a, b). Currently, three primary approaches exist for managing these self-toxic substances: physical, chemical, and biological methods. While the first two approaches require considerable energy and may cause secondary pollution, biological methods offer advantages such as effectiveness, practicality, and environmental friendliness. Biological control primarily involves the use of biocontrol bacteria or enzyme preparations; however, the processes of screening suitable biocontrol bacteria are complex, and their performance is often limited under extreme environmental conditions (Bao et al. 2022). Consequently, a significant research gap remains in the degradation of ferulic acid autotoxins, which necessitates the development of targeted and widely adaptable enzyme-based biocontrol technologies for efficient degradation of these self-toxic substances, particularly true for ferulic acid.

Enzymes serve as critical catalysts in biological systems. Compared with traditional inorganic catalysts, enzymes exhibit advantages such as biodegradability, specificity, low toxicity, mild reaction conditions, and environmental friendliness (Adeel et al. 2018; Cuprys et al. 2020). Among oxidases such as lignin peroxidase (LiP), manganese peroxidase, laccase, and horseradish peroxidase (HRP), LiP has poor temperature stability and is prone to inactivation (Biko et al. 2020). Furthermore, manganese peroxidase has a high production cost and is not suitable for large-scale applications. Laccase

relies on a copper ion active center and has a weak oxidation capacity (Bhardwaj et al. 2022). HRP consists of an enzyme protein and iron porphyrin prosthetic group, with a molecular weight of approximately 40,000 Da. HRP utilizes hydrogen peroxide (H_2O_2) as the electron acceptor in the following catalytic mechanism: H_2O_2 is efficiently decomposed through the Fe(III)/Fe(IV) cycle at the active center. The generated ·RO radicals can not only trigger the self-polymerization of pollutants (forming covalent coupling products with C–C, C–O–C, or C=C bonds) but also directly mineralize small organic molecules via electron transfer (Morsi et al. 2020). HRP exhibits considerable potential for degrading organic pollutants, including phenols, dyes, and pharmaceuticals, with remarkably high catalytic efficiency (Aldhahri et al. 2021; Bilal et al. 2022; B. Chen et al. 2021a, b), For instance, within 60 min, the degradation rate of phenol reaches 85.3% (Li et al. 2024), and with a H_2O_2 concentration of 13.4 mM, the removal rate of 2-methyl-6-ethylbenzidine reaches up to 97.6% (Shen et al. 2019).

The catalytic activity of free HRP is affected by pH, temperature, storage time and temperature, and reusability. Immobilized HRP can enhance stability and tolerance, preserve enzyme activity and reusability, and reduce application costs (Zdarta et al. 2019). Crosslinking is a key method for enzyme immobilization, whereby enzymes are combined with the functional groups on carriers to form stable covalent bonds. This approach allows for high enzyme loading, low leakage rates, strong environmental adaptability, and improved performance (Silva et al. 2022). However, the carrier choice considerably affects the enzyme's loading efficiency and stability. Common carriers, such as calcium alginate, chitosan, and nanoparticles, often require complex preparation processes (Bilal and Iqbal 2019; Zdarta et al. 2018). Biochar (BC) is an efficient, cost-effective, and environmentally friendly material with (i) a rich porous structure and high specific surface area that provide sufficient loading sites for enzymes, (ii) oxygen-containing surface functional groups (e.g., carboxyl and hydroxyl groups) that allow for formation of stable covalent bonds with enzymes, and (iii) good chemical stability and biocompatibility that effectively protect enzyme activity and improve the physical and chemical properties of soil (Wang et al. 2024). In addition, BC exerts a mitigating effect on soils under continuous crops (Cao et al. 2022; Feng et al. 2024; Han et al. 2019). Moreover, its surface morphology can be further optimized through acid–base modification or molten salt methods to enhance enzyme loading capacity (Wang et al. 2022). In particular, alkali modification can substantially increase its specific surface area and oxygen-containing functional groups compared with acid modification and molten salt methods (Liu et al. 2020; Zeng et al. 2023).

Continuous cropping is a major challenge to the sustainable development of the pepper industry, as the core issue lies in the continuous accumulation of phenolic acid autotoxic substances in soil. To address this problem, this study hypothesized that alkaline etching can considerably increase the specific surface area and the number of active sites of BC, effectively enhancing HRP immobilization. Furthermore, the immobilized HRP system constructed based on glutaraldehyde crosslinking exhibited superior catalytic performance compared with free enzymes, including a wider pH/temperature adaptation range and an efficient degradation ability for phenolic acid substances such as ferulic acid. Additionally, the immobilized HRP–CBC system considerably reduced the accumulation of toxic intermediate products via enzyme–carrier synergy and maintained stable degradation activity during repeated use. This research thus proposes an efficient and stable new strategy for enzyme immobilization to address the continuous cropping obstacle of pepper.

2 Materials and methods

2.1 Materials

Tobacco stems were obtained from a tobacco-growing area in Yunnan Province, China. HRP (> 250 units mg^{-1}), ferulic acid (FA; 99%), and disodium hydrogen phosphate (Na_2HPO_4; 99.99%) were obtained from Shanghai Aladdin Bio-Chem Technology Co., Ltd. Potassium hydroxide (KOH; 99.99%), potassium citrate ($C_6H_5K_3O_7$; 98%), potassium carbonate (K_2CO_3; 99%), sodium dihydrogen phosphate (NaH_2PO_4; 99%), glutaraldehyde (GA; 50% H_2O), Coomassie Brilliant Blue G250, 4-aminophenazone (4-AAP; 98%), phenol (C_6H_6O; 99.6%), vanillic acid (HVA; 98%), cinnamic acid (TC; 99%), coumalic acid (CA; 97%), and p-hydroxybenzoic acid (HBA; 99.5%) were provided by Shanghai Maclin Biochemical Co., Ltd. Methanol (CH_3OH; high-performance liquid chromatography (HPLC) grade) was provided by Merck, Germany. H_2O_2 (30%) and nitric acid (HNO_3; 85%) were provided by China National Pharmaceutical Group Chemical Reagent Co., Ltd. Deionized water (Merck Millipore Milli-Q EQ 7008) was used in all experiments.

2.2 Preparation and stability testing of immobilized enzyme materials

2.2.1 Preparation, functionalization and enzyme immobilization of modified biochar

Tobacco stems were air-dried, ground, and sieved before being heated in a muffle furnace to produce BC. Subsequently, BC was (i) soaked in a K_2CO_3 solution, (ii) dried,

and (iii) calcined in a muffle furnace for 2 h, followed by washing to obtain carbonate-modified BC (CBC). BCs prepared by replacing K_2CO_3 with KOH and $C_6H_5K_3O_7$ were named potassium hydroxide-modified BC (KBC) and potassium citrate-modified BC (NBC), respectively. Furthermore, BC was (i) immersed in HNO_3, (ii) washed, (iii) dried, and (iv) incubated in phosphate-buffered saline for 24 h. Thereafter, an equal volume of GA was added for crosslinking, followed by thorough washing and drying (Petronijević et al. 2021a). The resulting BC was mixed with HRP and dried at room temperature to produce HRP–BC. The enzymes immobilized on CBC, KBC, and NBC were designated as HRP–CBC, HRP–KBC, and HRP–NBC, respectively. Detailed preparation procedures are provided in Supplementary File S1.

2.2.2 Enzyme loading and enzyme activity tests of the immobilized enzymes

The total protein content of immobilized enzymes was quantified using the Coomassie Brilliant Blue method (Chen et al. 2024), The HRP concentration in the solution before and after immobilization was measured at 595 nm using an ultraviolet-visible spectrophotometer (TU-1810D, China). The loading capacity of the immobilized enzyme was calculated using Eq. (1). Enzyme activity was defined as the amount of HRP required to decompose 1 μmol of H_2O_2 per min under standard conditions. For activity assays, 0.1 mL of free HRP or 25 mg of immobilized HRP was added to a mixture containing 1.4 mL of 4-AAP solution and 1.5 mL of H_2O_2 solution. The reaction time was set to 1 min for free HRP and 5 min for immobilized HRP. Absorbance was recorded at 510 nm, and the enzyme activities of free HRP and immobilized HRP were calculated using Eq. (2) (Besharat et al., 2018). The maximum activity of free HRP and immobilized HRP was normalized to 100%, and the relative enzyme activity under other conditions was calculated by comparing their respective activities with this reference value using Eq. (3).

$$Q = \frac{(C_0 - C_1)v}{m} \times 100\% \quad (1)$$

$$\text{Enzyme activity (U/mg)} = \frac{E_{510} \times V}{6.58 \times M \times T} \quad (2)$$

$$\text{Relative enzyme activity (\%)} = \frac{A}{A_{max}} \times 100\% \quad (3)$$

In the aforementioned equations, q denotes the enzyme loading capacity (mg g^{-1}), C_0 is the initial concentration of the enzyme solution (mg mL^{-1}), C_1 is the enzyme concentration in the solution after immobilization (mg mL^{-1}), v is the volume of the solution (mL), m is the mass of the material (g), E_{510} is the change in absorbance at 510 nm, V is the reaction volume of the solution (mL), M is the mass of the enzyme (mg), T is the reaction time (min), A is the enzyme activity (U mg^{-1}), and A_{max} is the maximum enzyme activity of free HRP or immobilized HRP.

2.2.3 Determination of the kinetic constants for HRP and HRP–CBC

The kinetic parameters, Michaelis–Menten constant (K_m), and maximum reaction velocity (V_{max}) of free HRP and immobilized HRP were determined by varying the H_2O_2 concentration (0.1–5.0 mM) and measuring the enzymatic activity. These parameters were calculated using the Michaelis–Menten model and Lineweaver–Burk linearization.

$$\frac{1}{V_0} = \frac{K_m}{V_{max}} \times \frac{1}{[S]} + \frac{1}{V_{max}}$$

In the aforementioned formula, V_0 is the initial rate of the reaction (mM min^{-1}), V_{max} is the maximum rate of the reaction (mM min^{-1}), K_m is the Michaelis constant (mM), and *[S]* is the initial ABTS concentration (mM).

2.2.4 Determination of the stability of immobilized enzymes

The enzymatic activities of free and immobilized HRP in 50 mM PBS buffer were analyzed at various pH levels (3, 4, 5, 6, 7, and 8) and temperatures (20 °C, 30 °C, 40 °C, 50 °C, 60 °C, and 70 °C) to evaluate their pH and thermal stability. Free HRP and immobilized HRP were stored at 4 °C and 25 °C for 30 days, and enzymatic activity was measured every 5 d to assess long-term storage stability. The enzymatic activity of immobilized HRP was determined after seven consecutive uses to evaluate its recyclability (Jing et al. 2025).

2.3 Determination of the degradation rates of autotoxic substances

2.3.1 Degradation of autotoxic substances

A series of FA solutions (3 mL) with specific concentrations was prepared. Then, a defined amount of immobilized HRP or an equivalent amount of free HRP was added to each solution. The effects of pH (5.0–8.0), solution temperature (25–55 °C), initial FA concentration (20–70 mg L^{-1}), material dosage (1–10 U mL^{-1}), H_2O_2 concentration [c(H_2O_2):c(FA) ratio: 0.15–1.0], and reaction time (1–24 h) on FA degradation were systematically investigated. In all experiments, only one parameter was varied, while the other parameters were kept constant. Each experiment was repeated three times to ensure reliability. In the cyclic degradation test of 20 mg L^{-1} FA using immobilized HRP, the supernatant was collected

at the end of each cycle and filtered through a 0.22 μm membrane to determine the FA removal efficiency. The immobilized HRP was rinsed twice with 50 mM PBS (pH 7.0) and reused in the subsequent cycle. For the degradation of multiple phenolic acid autotoxic substances, 3 mL of HVA, TC, CA, and HBA solutions (concentration = 20 mg L^{-1}) were prepared. Both 2 U mL^{-1} of free HRP and an equivalent amount of immobilized HRP were added separately. The mixtures were incubated at 30 °C for 2 h under shaking at 180 rpm for 2 h. Subsequently, the supernatants were collected and filtered through a 0.22 μm membrane. The removal rates were quantified via HPLC (HPLC-Agilent 1260, USA). Additionally, the mineralization degree of FA was analyzed using a total organic carbon (TOC) analyzer (Shimadzu TOC-L, Japan).

2.3.2 Capsicum seed germination experiment

Plump and uniformly sized capsicum seeds were selected, soaked in a 3% sodium hypochlorite solution for 5 min and rinsed five times with distilled water. Three layers of qualitative filter paper were placed flat in each Petri dish, and 30 seeds were evenly distributed on itthe paper. Subsequently, 5 mL of FA solution (20 mg L^{-1} FA solution) was added to each dish; then, the dishes were covered and placed in an incubator at 30 °C for 10 days. The filter paper was kept moist during the seed germination period. The germination rate was calculated when the seedlings reached 1 mm in length, and root lengths were measured. Germination tests were simultaneously conducted using FA solutions treated with immobilized HRP for 6 h, with distilled water serving as the control. All treatments were repeated three times. The concentration of exogenous FA added to the soil was 20 mg L^{-1}. On the 7th, 9th, and 11th days, the supernatant was extracted with NaOH and the pH was adjusted to 2.8. The solution was then filtered through a 0.22 μm filter membrane and analyzed via HPLC (HPLC-Agilent 1260, USA).

2.4 Material characterization and elucidation of degradation pathways and mechanisms

The N_2 adsorption–desorption isotherms at 77 K liquid nitrogen were measured using a fully automatic specific surface area and porosity analyzer (BET Micromeritics ASAP 2460 USA) to determine the specific surface area and pore size of the material. The surface morphology of the material was observed via field-emission scanning electron microscopy (SEM; Zeiss Gemini 300 Germany) and the surface element distribution was analyzed via energy dispersive spectrometry (EDS; Zeiss Gemini 300 Germany). Electron spin resonance (ESR) spectra were recorded at 3460–3560 G using an electron spin resonance spectrometer (Bruker EMXplus-6/1, Germany). The surface functional groups of the material were analyzed via Fourier transform infrared (FTIR) spectroscopy (Thermo Fisher Nicolet iN10). Degradation intermediates were tested via HPLC–coupled with quadrupole time-of-flight mass spectrometry (Agilent 1290-6550). The toxicity of FA and its intermediates was evaluated using the ECOSAR software.

2.5 Data processing and statistical analysis

Data and graphs were processed using Excel 2021 and Origin 2021, respectively. Data are presented as the mean ± standard error of three replicates. One-way ANOVA was used to compare the differences among different treatment groups. If significant differences were found among the groups ($p < 0.05$), post hoc multiple comparisons were conducted using the least significant difference method and the Waller–Duncan method. Capital letters (A, B, and C) indicate significant differences among different treatment groups of the same material, while lowercase letters (a, b, c) indicate significant differences among different materials under the same conditions. All data were tested for normal distribution and homogeneity of variance before analysis. If the data did not meet the conditions for parametric tests, the Kruskal–Wallis non-parametric test was used . All statistical analyses were performed using DMASA 2024 software, and the statistical significance level was set at 0.05. The ecological toxicity of FA and its intermediate products was evaluated using ECOSAR software.

3 Results and discussion

3.1 Physicochemical characteristics of horseradish peroxidase immobilized on modified biochar

The impacts of three types of alkali etching on the surface morphology of BC are presented in Table S1. The specific surface area exhibited a decreasing trend as follows: CBC > NBC > KBC > BC. Notably, CBC had the largest pore diameter and volume. This can be attributed to the reaction of K^+ with the glycosidic bonds in cellulose polysaccharide units at high temperatures, along with the gas expansion effect caused by CO_2 and CO generated from CO_3^{2-} (Ji et al. 2021; Zhao et al. 2024). After alkali treatment, the adsorption–desorption isotherms of BC transitioned from Type I to Type IV with an H4 hysteresis loop (Fig. 1a). The pore diameters of the three alkali-modified BCs corresponded to those of microporous and mesoporous materials (Fig. 1b). After immobilization, the pore diameter increased from 2.1 to 4.0 nm. HRP was selectively adsorbed at the entrance or on the outer surface of the micropores through noncovalent forces such as electrostatic adsorption, hydrophobic interactions, and hydrogen bonding, which might cause HRP to cover the micropore openings, thereby blocking

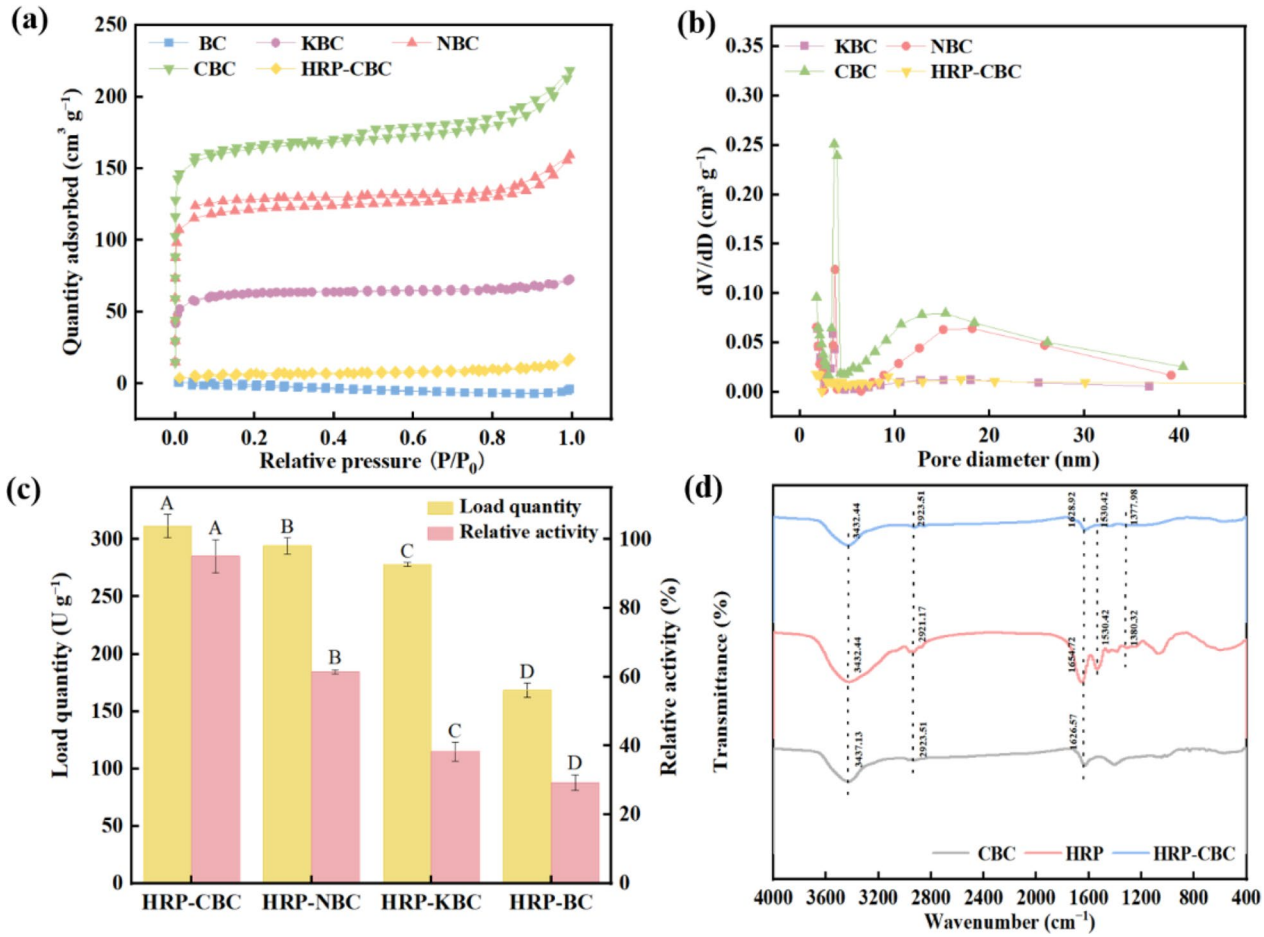

Fig. 1 **a**, **b** Pore size distribution and adsorption–desorption isotherms of BC, CBC, NBC, KBC and HRP–CBC; (**c**) Horseradish peroxidase loading and enzyme activity on biochar prepared using different alkali treatments; (**d**) The FTIR spectra of CBC, HRP and HRP–CBC. Differences among HRP–CBC, HRP–NBC, HRP–KBC, and HRP–BC are indicated by capital letters ($p < 0.05$)

nitrogen adsorption and leading to increased average pore diameter. Alternatively, laccase might be densely immobilized on the surface of the micropore-rich region, indirectly "occupying" the micropores, increasing the average pore diameter after CBC immobilization of HRP (Table S1) (Chen et al. 2024). Furthermore, an increase in pore size improves water retention and permeability, increasing water availability to plants (Ng et al. 2022). Enzyme loading capacity and relative enzyme activity are critical indicators of loading concentration and post-loading enzyme activity (Fig. 1c). Among the samples, HRP–CBC exhibited the highest enzyme loading capacity (311.46 U g^{-1}) and relative enzyme activity, followed by HRP–NBC, HRP–KBC, and HRP–BC in a descending order. Enzyme loading capacity and enzyme activity are strongly correlated with the carrier's specific surface area, pore diameter, and pore volume (Maryskova et al. 2019). The covalent crosslinking of HRP and the remaining GA on the CBC surface might explain the 96.84% reduction in the specific surface area of HRP–CBC compared with that of CBC (Taheran et al. 2017), a result in alignment with the BET analysis results. Table S2 summarizes the relevant literature on the loading capacity of immobilized HRP. As can be seen in this table, the enzyme immobilization method adopted in this study achieved a higher loading capacity.

The FTIR spectra of CBC, HRP, and HRP–CBC are shown in Fig. 1d. The peaks observed at 3437, 2921, and 1401 cm^{-1} correspond to the O–H bond of hydroxyl groups, the C–H bond of aromatic rings, and the C=C stretching vibration, respectively (Liu et al. 2021; Naghdi et al. 2018; Yang et al. 2024). For HRP–CBC, the peaks observed at 1377 and 1183 cm^{-1} are attributed to the C–N stretching vibrations of amine groups (Imam et al. 2021), while that observed at 1530 cm^{-1} corresponds to the amide I band of proteins (Petronijević et al. 2021a), The presence of the characteristic HRP peaks confirms its successful immobilization onto the

carrier (Liu et al. 2023). The SEM images of the three materials (Fig. 2) revealed uniformly distributed pores across the BC surface. In comparison, the pores on the CBC surface were deeper and exhibited larger diameters due to K_2CO_3-induced erosion of the carbonaceous structure (Petronijević et al. 2021a). Notably, the HRP–CBC surface displayed aggregated enzymes forming a thick enzyme coating (Fig. 2d, e), further corroborating the successful enzyme immobilization (Hoinacki et al. 2022; Rasheed et al. 2024). EDS analysis (Fig. 2c, f) and elemental mapping (Fig. 2g–l) results confirmed that HRP was successfully immobilized on the CBC carrier. The mass ratio of N in HRP–CBC was 5.7 times that in CBC, mainly due to the contribution of peptide bonds, R groups, and free amino groups present in the HRP molecule (Kumar et al. 2019). The relative contents of O and N considerably increased after immobilization and showed an unevenly dispersed spatial distribution on the carrier surface (Sanroman et al. 2020). These results collectively demonstrate effective HRP immobilization, which is consistent with the BET and FTIR findings.

3.2 Stability of immobilized horseradish peroxidase

The acid–base stabilities of HRP and HRP–CBC are presented in Fig. 3a. Both enzymes exhibited maximum activity at pH 7.0, decreasing when the solution pH deviated from this optimal value. This finding aligns with Chen's (2020) conclusion. The enzyme activity of

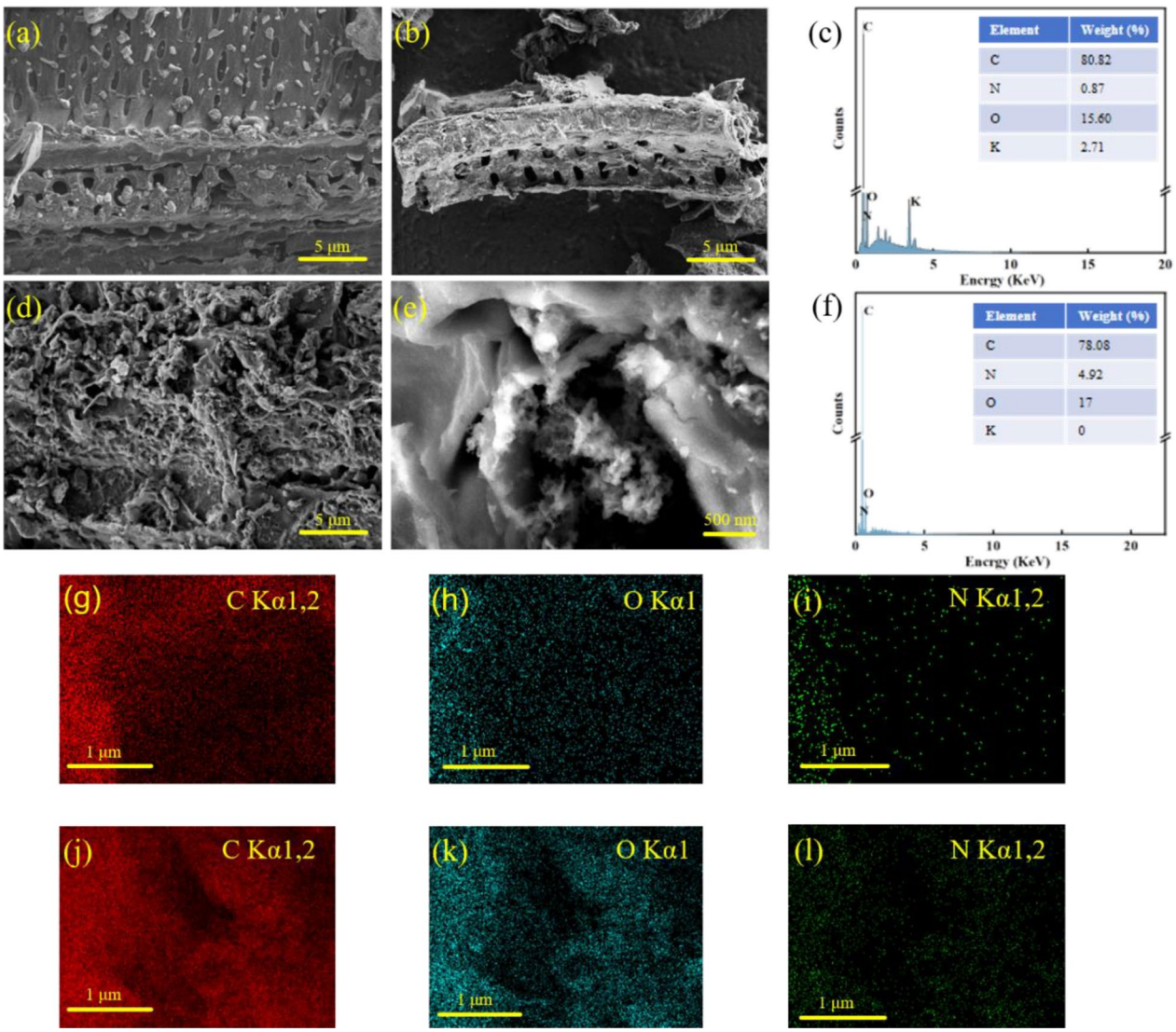

Fig. 2 Representative SEM images and element distribution of BC (**a**), CBC (**b**, **c**) and HRP–CBC (**d**–**f**). C, O and N elemental mapping images of CBC (**g**–**i**) and HRP-CBC (**j**–**l**)

HRP–CBC was comparable to that of free HRP under acidic conditions. However, under alkaline conditions, HRP–CBC demonstrated superior stability than free HRP owing to the buffering effect of the functional groups embedded within the biochar matrix. These functional groups mitigated the extreme pH fluctuations in

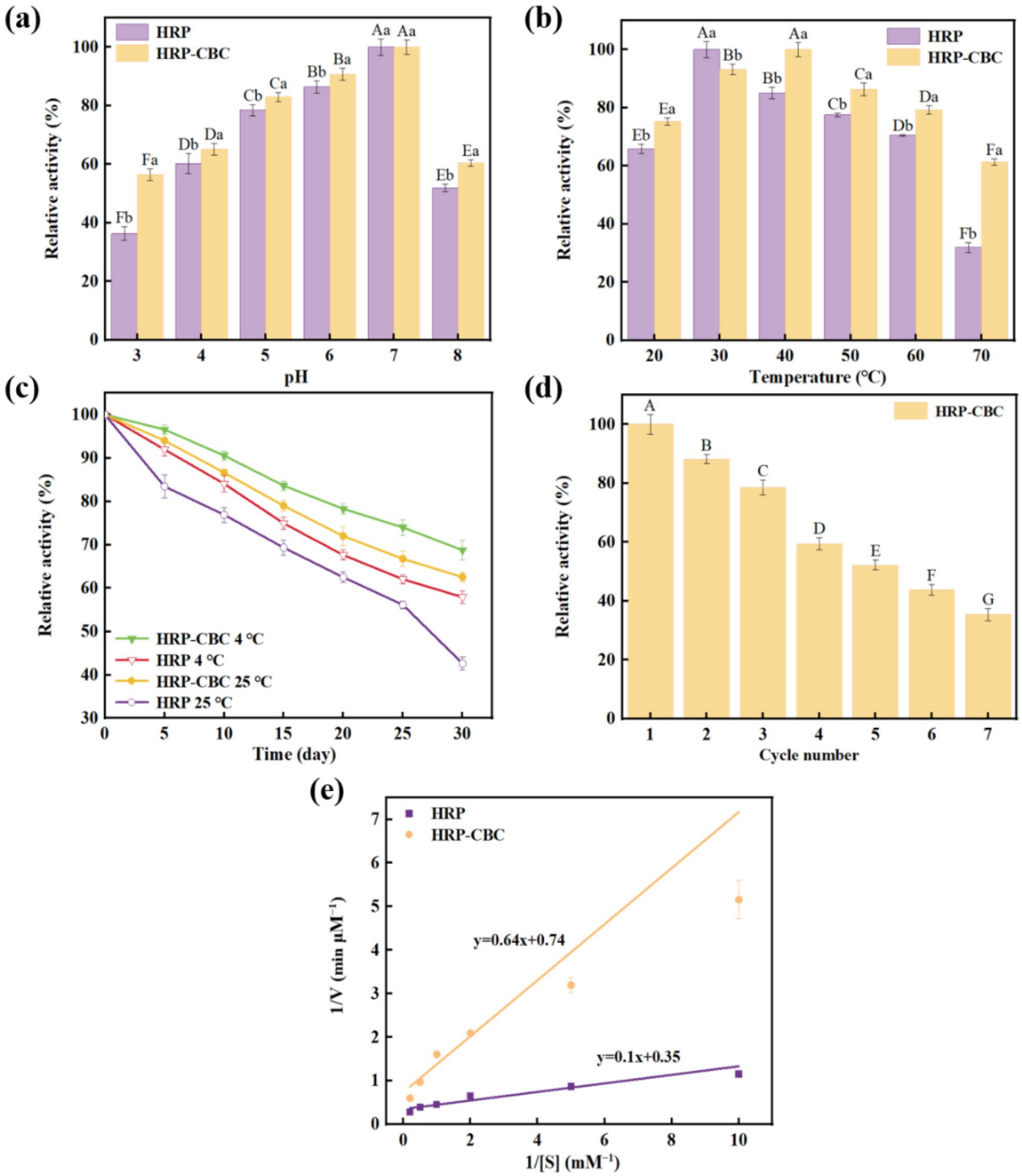

Fig. 3 Stability of free horseradish peroxidase and HRP–CBC: (**a**) pH, (**b**) temperature, and (**c**) storage time; (**d**) HRP–CBC reusability; (**e**) kinetic parameters of HRP and HRP–CBC. [enzyme dosage = 2 U mL^{-1}, biochar dosage = 8 mg mL^{-1}, temperature = 35 °C, and pH = 7. Capital letters indicate differences between HRP and HRP–CBC samples, and lowercase letters indicate the differences in pH and T ($p < 0.05$)]

the microenvironment surrounding HRP–CBC, thereby reducing the adverse effects of pH on enzyme activity (Petronijević et al. 2021a). Liu et al. (2023) demonstrated that HRP exhibits substantial reduction in enzymatic activity under alkaline conditions, a finding that aligns with the results of this research. The temperature stability data for HRP and HRP–CBC are shown in Fig. 3b. The optimal temperatures for relative enzyme activity were 30 °C for HRP and 40 °C for HRP–CBC. Notably, both enzymes exhibited a rapid decrease in activity with increasing temperature due to thermal-induced denaturation of the enzyme structure. At 70 °C, HRP–CBC retained 61.4% of the relative enzyme activity, whereas free HRP retained only 31.9%. The enhanced thermal stability of HRP–CBC can be attributed to the protective framework provided by CBC, which minimizes the impact of high-temperature exposure on the 3D structure of the enzyme (Almulaiky et al. 2019; Besharati Vineh et al. 2018). The relative activity in response to pH and temperature changes also showed the same trend over 30 days (Fig. S1). These findings indicate that CBC is an effective carrier that maintains HRP activity and conformation under fluctuating temperature conditions. Under normal storage conditions, HRP exhibits instability (Wu et al. 2023). However, as depicted in Fig. 3c, after 30 days of storage, HRP–CBC retained 68.8% and 57.9% of relative activity at 4 °C and 25 °C, respectively, compared with 62.5% and 42.6% for free HRP. This corresponds to an 11–20% improvement in relative enzyme activity, likely due to charge neutralization from the interactions between HRP and CBC, increasing the resistance of the immobilized enzyme. As shown in Fig. 3d, the relative activity of HRP–CBC decreased to 35.4% after seven cycles, which is to the leaching of noncovalently bound enzymes during repeated washing, prolonged exposure of the enzyme to H_2O_2, and loss of carrier material (Alshawafi et al. 2018). Compared with free HRP, the K_m of HRP–CBC increased (Fig. 3e, Table S3), indicating a lower affinity for the substrate. This might be due to the carrier hindering contact between the enzyme and substrate. The decrease in V_{max} might result from spatial hindrance of the carrier during HRP immobilization on the CBC carrier, which impedes the mass transfer of the substrate, or from conformational changes in the enzyme's active center induced by the immobilization force (Weber et al., 2023b; Wu et al. 2023).

3.3 Effects of immobilized horseradish peroxidase on phenolic acid autotoxic substance degradation

Based on the typical soil pH range, the impact of pH on FA removal by HRP, HRP–BC, and HRP–CBC was assessed within a range of 5.0–8.0 (Fig. 4a). The FA removal efficiency of HRP–CBC was significantly higher than that of the other two materials ($P p < 0.05$), suggesting that alkaline etching enhances enzyme immobilization and improves phenolic acid removal. The highest FA removal rate for all three materials was observed at a solution pH of 7.0, consistent with the optimal catalytic pH of HRP. When the pH was excessively high or low, the FA removal rate decreased for all three materials. This is attributed to changes in H^+ and OH^- concentrations, which alter the protein structure and surface interactions of pollutants, thereby affecting the enzymatically active conformation and chemical interactions (Bilal et al. 2019). Figure 4b illustrates the effects of HRP, HRP–BC, and HRP–CBC on FA removal at different temperatures. Within the 25–55 °C range, FA removal efficiencies followed the trend HRP–CBC > HRP–BC > HRP, indicating that enzyme immobilization considerably enhances the thermal stability of HRP. At 35 °C, the FA removal rates for HRP–BC and HRP–CBC reached their peaks before declining. Further increases in temperature resulted in denaturation, leading to changes in the conformation of active sites, loss of binding affinity between pollutants and active sites, and a subsequent decrease in degradation efficiency (Kalsoom et al. 2023). Upon increasing the enzyme dosage from 1 to 10 U mL^{-1}, the FA removal rates of the three materials ($p < 0.05$). In particular, the removal rate of HRP–CBC increased from 54.2% to 79.5% (Fig. 4c). This improvement can be attributed to the increase in the number of catalytic oxidation active sites with increasing immobilized enzyme dosage. The overall removal rates for initial FA concentrations ranging from 20 to 70 mg L^{-1} followed the trend HRP–CBC > HRP–BC > HRP (Fig. 4d), with significant differences among treatments ($P < 0.05$). Furthermore, the removal rates of all three materials gradually decreased with increasing initial FA concentration owing

(See figure on next page.)

Fig. 4 Effects of different parameters on FA degradation efficiency for HRP, HRP–BC, and HRP–CBC. **a** pH, (**b**) temperature, (**c**) initial FA concentration, (**d**) biocatalyst dosage, (**e**) c(H_2O_2):c(FA), (**f**) time, (**g**) kinetic models, (**h**) TOC, (**i**) HRP–CBC and HRP–BC reusability, (**j**) pollutant (Conditions: initial concentration = 20 mg L^{-1}, enzyme dosage = 2 U mL^{-1}, HRP–CBC = 8 mg mL^{-1}, HRP–BC = 12 mg mL^{-1}, temperature = 35 °C, pH = 7, H_2O_2 = 0.5 mM, TC, CA, HBA and HVA concentration = 20 mg L^{-1}). **k** Impact of capsicum seed germination and root length (Time = 10 d), (**l**) soil degradation experiment. Capital letters indicate differences among samples of FA substances of HRP, HRP–BC, and HRP–CBC, while lowercase letters represent differences among pH, T, FA concentration, material dosage, H_2O_2 concentration, and treatment groups ($p < 0.05$)

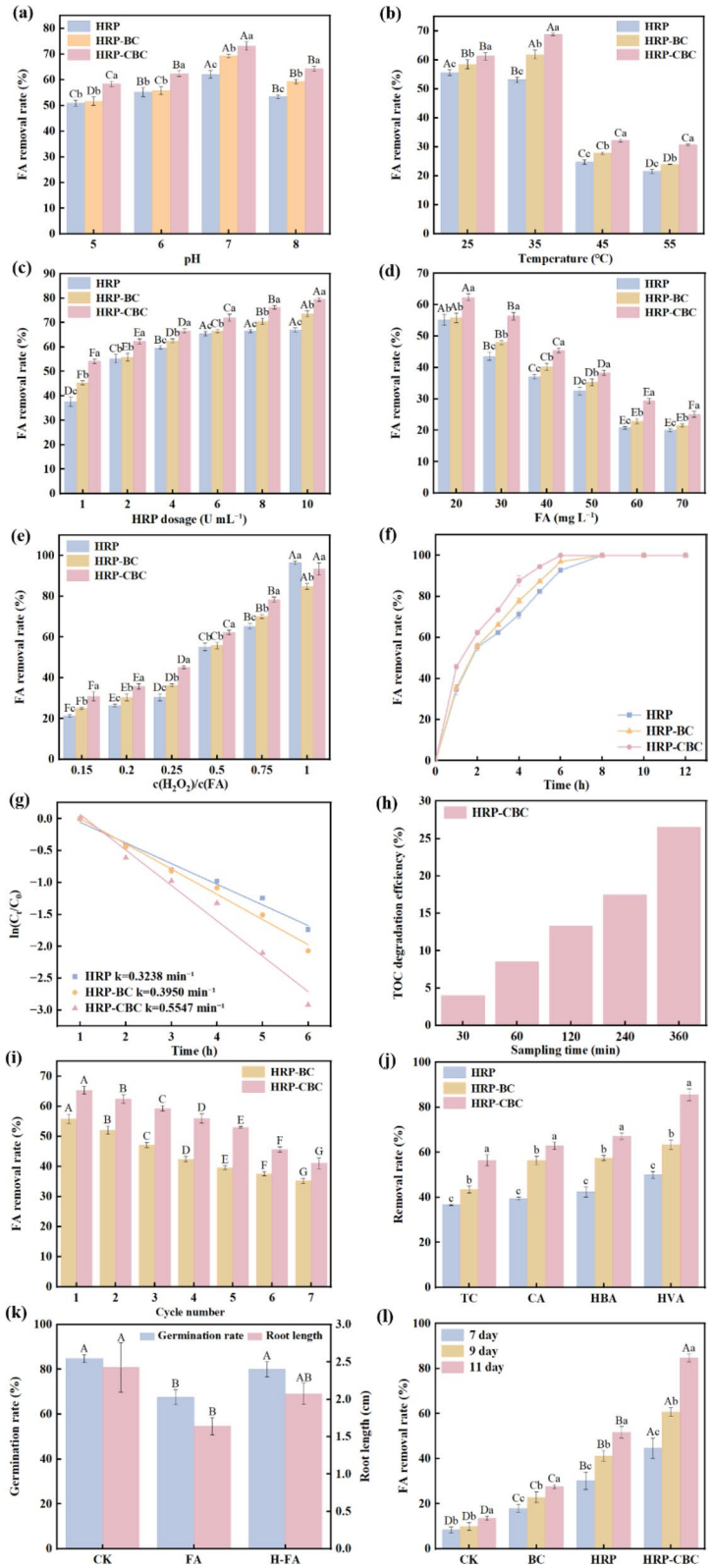

Fig. 4 (See legend on previous page.)

to excessive accumulation of pollutant molecules and the formation of intermediates, which limited the accessibility of enzyme active sites (Chen et al. 2024). In enzymatic reactions, H_2O_2 serves as a co-substrate to activate HRP and thereby enhances the catalytic efficiency. When the $c(H_2O_2)/c(FA)$ ratio increased from 0.15 to 1, the FA removal rates for HRP, HRP–BC, and HRP–CBC gradually increased from 20–30% to 85–97% (Fig. 4e). With a further increase in H_2O_2 concentration, HRP continued to be activated, enabling the oxidation of the remaining pollutants (Petronijević et al. 2021a). The removal efficiencies of the three materials generally followed the trend HRP–CBC > HRP–BC > HRP, further highlighting the advantage of enzyme immobilization in maintaining activity. Notably, the removal rate of free HRP reached its maximum only when the $c(H_2O_2)/c(FA)$ ratio reached 1, owing to the increased direct contact between high-concentration H_2O_2 and free HRP, which considerably reduced mass transfer resistance and increased HRP activation (Yang et al. 2024). Therefore, the FA removal rates of HRP, HRP–BC, and HRP–CBC gradually decreased as the reaction proceeded and the substrate concentration decreased (Fig. 4f). HRP–CBC achieved a 100% FA removal rate at 6 h, 2 h earlier than HRP and HRP–BC, thus showing the fastest FA removal rate. This might be due to substrate enrichment in the pores of HRP–CBC, which increased the contact between the substrate and enzyme (Chen et al. 2024). The FA removal reaction rates followed the order HRP–CBC > HRP–BC > HRP. In particular, the kinetic constant k for FA removal by HRP–CBC was 1.4 and 1.7 times higher than that by HRP–BC and HRP, respectively (Fig. 4g) (Yang et al. 2024). The degree of TOC mineralization is shown in Fig. 4h. During FA degradation by HRP–CBC from 30 to 360 min, the TOC mineralization rate gradually increased, indicating that the intermediate organic products decreased as the reaction proceeded. HRP–CBC exhibited a significantly higher FA removal rate. Reusability is a key advantage of immobilized enzymes over free enzymes. As the number of reuse cycles increased from 1 to 7, the FA removal rates for HRP–CBC and HRP–BC gradually decreased from 65.3% and 55.8% to 41.1% and 35.2%, respectively (Fig. 4i); however, both materials maintained relatively high enzyme activity throughout the process. The reduction in enzyme activity or enzyme leakage may be attributed to factors such as repeated washing, accumulation of free radicals, and blocking of active sites by the degradation products (Weber et al. 2023), Overall, HRP–CBC demonstrated superior reusability compared with HRP–BC and HRP–BC. The removal efficiencies for the four phenolic acids followed the order HRP–CBC > HRP–BC > HRP (Fig. 4j), with statistically significant differences among treatments ($p < 0.05$). Within 2 h, HPR–CBC achieved > 50% removal rates for TC, CA, HBA, and HVA, demonstrating its broad applicability to various phenolic acid pollutants. Table S2 compares multiple studies on immobilized HPR for organic pollutant degradation, including enzyme loading capacity, degradation efficiency, reusability, and operational stability. The results demonstrate that HPR–CBC exhibited strong stability, stress resistance, broad application potential, and high degradation efficiency.

The effects of FA solution treatment on chili seed germination before and after the process are presented in Fig. 4k and Fig. S1. Seeds treated with distilled water exhibited the highest germination rate and root length. After soaking in the FA solution, the germination rate decreased significantly by 17% and the root length decreased by 0.79 cm. However, when seeds were soaked in the FA solution and subsequently treated with HRP–CBC, the germination rate and root length restored to levels not significantly different from those corresponding to the control treatment. These results indicate that HRP–CBC effectively alleviates the inhibitory effects of soil allelochemical FA on capsicum seed germination and root growth. Figure 4l shows the FA degradation in soil for HRP–CBC on the 7th, 9th, and 11th days. On the 11th day, the FA degradation rate by HRP–CBC was 84.68%, indicating its HRP–CBC potential for practical soil applications. However, this study only investigated the short-term (11 day) degradation effects. Future research should conduct longer-term soil experiments (e.g., 30–90 days), further evaluate the impact on microbial communities, and perform field validation to comprehensively assess the applicability and stability of HPR-CBC in real soil environments.

3.4 FA degradation pathway and toxicity assessment of intermediate products

TEMP and DMPO were used as free radical spin traps for ESR analysis of the reaction system to verify the charge transfer mechanism and free radical capture efficiency (Fig. 5a–c). The spectra showed DMPO–·OH with a typical 1:2:2:1 quadruple peak structure, TEMP–$^1O_2$ with a 1:1:1 triple peak feature, and DMPO–$\cdot O_2^-$ with its characteristic 1:1:1 signal peak, confirming the generation of reactive oxygen species (·OH, $^1O_2$, and $\cdot O_2^-$) during the reaction. The quenching experiment confirmed the existence of three active species (Fig. S3). This indicates that OH, $^1O_2$, and $\cdot O_2^-$ jointly contributed to FA degradation by the HRP–CBC system and that radical and nonradical pathways coexisted. Figure 5d shows the linear sweep voltammetry (LSV) curves of HRP, HRP–CBC, and BC. HRP–CBC has a larger arc diameter than HRP and BC, implying that the charge transfer rate of HRP–CBC is higher than that of HRP and BC.

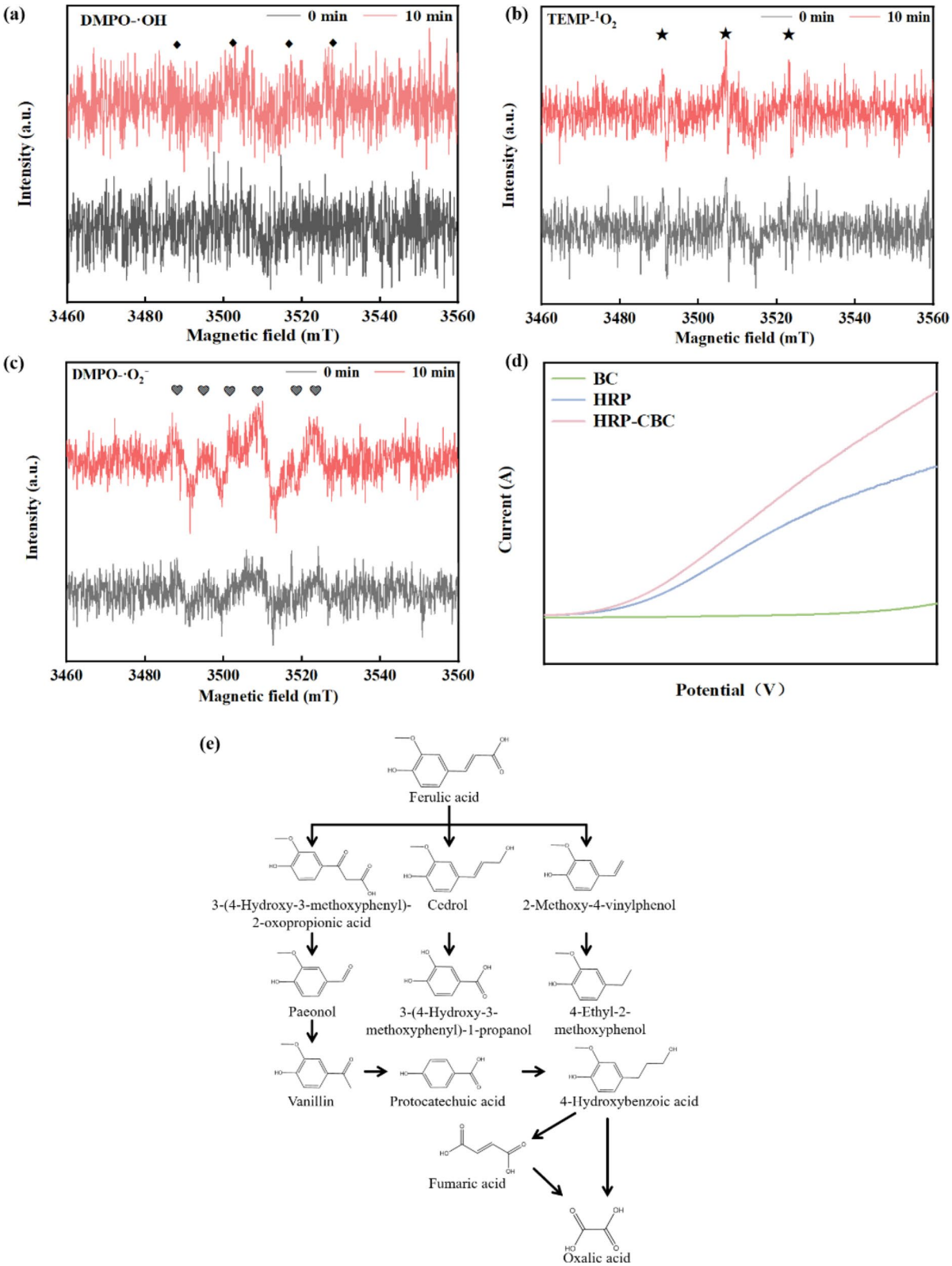

Fig. 5 **a**–**c** ESR analysis results, (**d**) LSV curves, and (**e**) mechanism of FA degradation under HRP–CBC

Liquid chromatography–mass spectrometry (LC–MS) was employed to identify the intermediate products of the catalytic reaction, providing insights into the underlying degradation pathway and mechanism (Fig. 5c). As can be seen in Fig. 5c, H_2O_2 accepts electrons from HRP and reduces to water, while HRP is oxidized by H_2O_2 and loses electrons to form the intermediate Compound I. Subsequently, FA donates an electron to Compound I, leading to the formation of Compound II. FA loses electrons and forms different free radicals ·RO with different intermediate products R. Compound II is unstable and reduces to its initial enzyme form by accepting electrons from FA. Ultimately, FA oxidizes to the free radical ·RO and subsequently participates in enzymatic reactions, including rearrangement processes (Chen et al. 2024). There exist three degradation pathways. In the first pathway, FA reacts with ·OH via electrophilic addition to form 3-(4-hydroxy-3-methoxyphenyl)-2-oxopropionic acid. Subsequently, this acid undergoes oxidation to produce paeonol and vanillin. The methoxyphenyl group of vanillin is cleaved, and the H atom adjacent to the C=O bond is replaced by an OH, forming protocatechuic acid. Thereafter, a carboxyl group is eliminated to generate 4-hydroxybenzoic acid. Finally, the benzene ring is disrupted, leading to the formation of low-molecular-weight compounds such as fumaric acid and oxalic acid (Ren et al. 2019). The second pathway involves the reaction of FA with ·OH to form pinoresinol. Subsequently, the C=C double bond undergoes cleavage, resulting in the formation of 3-(4-hydroxy-3-methoxyphenyl)-1-propanol (Zhang et al. 2019); The third pathway involves the oxidation of FA by ·OH radicals to form 2-methoxy-4-vinylphenol. Subsequently, this compound undergoes C=C double bond cleavage, leading to the formation of 4-ethyl-2-methoxyphenol (Ren et al. 2023).

Figure 6 shows the acute and chronic toxicities of the intermediate products generated by HRP–CBC during FA degradation on fish, water fleas, and green algae. During FA degradation by HRP–CBC, some intermediate products showed varying degrees of toxicity. Overall, all products were transformed into low- or non-toxic substances (A: 3-(4-hydroxy-3-methoxyphenyl)-2-oxopropionic acid, B: paeonol, D: protocatechuic acid, F: fumaric acid, H: pinocembrin, I: 3-(4-hydroxy-3-methoxyphenyl)-1-propanol, and K: 4-ethyl-2-methoxybenzene). However, vanillin (C), 4-hydroxybenzoic acid (E), and oxalic acid (G) exhibited acute toxicity. As the reaction continued, the pollutants were continuously degraded, eventually achieving detoxification, indicating that HRP–CBC has high detoxification potential. The results are consistent with the TOC removal rate and seed germination rate (Fig. 4h). However, current research on the ecological

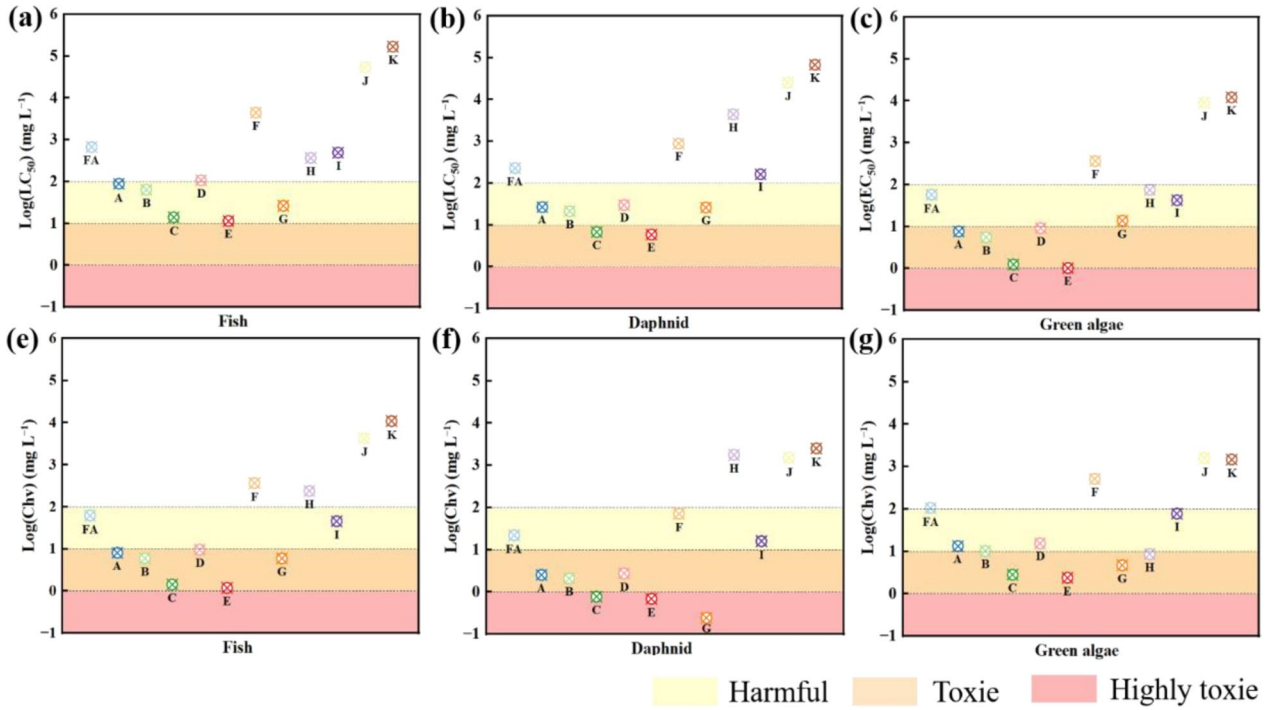

Fig.6 Biotoxicity assessment of FA and its intermediates. **a**–**c** acute toxicity; (**e**–**g**) chronic toxicity. (A: 3-(4-hydroxy-3-methoxyphenyl)-2-oxopropionic acid, B: paeonol, C: vanillin, D: protocatechuic acid, E: 4-hydroxybenzoic acid, F: fumaric acid, G: oxalic acid, H: pinocembrin, I: 3-(4-hydroxy-3-methoxyphenyl)-1-propanol, J: 2-methoxy-4-vinylphenol, K: 4-ethyl-2-methoxybenzene)

risk assessment of intermediate products still has limitations, lacking verification of microbial community toxicity and long-term bioaccumulation effects. Therefore, future studies should integrate microbial toxicity testing (e.g., soil enzyme activity, microbial diversity analysis) with pot or field-based plant experiments to more comprehensively evaluate the environmental safety of this technology.

4 Conclusion

BC enzyme carriers with a super-large specific surface area and pore structure were prepared via K_2CO_3 etching. The loading capacity and enzymatic activity of immobilized HRP were optimized using a crosslinking method, resulting in a maximum loading capacity of 311.46 U g^{-1}. Under different reaction conditions, we observed significant differences in the removal rates of FA for three materials (HRP, HRP–BC, and HRP–CBC). At 35 °C and pH 7, the FA removal rates achieved by HRP–CBC were the highest, reaching 68.8% and 73.1%, respectively. When using 2 U mL^{-1} HRP–CBC under pH 7, the removal rate of 20 mg L^{-1} FA reached 100% within 6 h. In addition, HRP–CBC demonstrated excellent degradation capability for multiple phenolic acids responsible for autotoxicity in pepper. The application of HRP–CBC to degrade FA removed the inhibitory effects on the germination rate and root length of pepper seeds under FA conditions. LC–MS and ecological toxicity analyses revealed that FA was degraded into smaller organic molecules with considerably lower toxicity. HRP–CBC exhibited superior stability, reusability, and stress resistance. Thus, HRP immobilization onto a modified BC offers a promising new approach for addressing phenolic acid autotoxic substances in continuous cropping systems. Future research should focus on conducting field soil experiments to systematically evaluate (i) the phenolic acid degradation efficiency of this technology in actual environments and (ii) its regulatory effect on crop growth for promoting the transformation of this green remediation technology from laboratory research to field application.

Supplementary Information

The online version contains supplementary material available at https://doi.org/10.1007/s42773-025-00512-9.

Supplementary Material 1.

Author contributions

Xueyan Zhang: writing—review & editing, writing—original draft, visualization, validation, methodology, investigation, formal analysis, data curation, conceptualization. Shiyu Lv: writing—review & editing, writing—original draft, visualization, validation, methodology, investigation, formal analysis, data curation. Tian Yuan: methodology, investigation, data curation. Kerong Fu: visualization, software, methodology, investigation, formal analysis. Pu Yang: data curation, formal analysis, writing—review & editing. Yanpo Yao: data curation, methodology. Junfeng Liang: writing—review & editing, validation. Tongguo Gao: supervision, resources, project administration. Feng Wang: writing—review & editing, supervision, resources, project administration, methodology, investigation, funding acquisition, conceptualization.

Funding

This work was supported by the National Key Research and Development Program of China [2022YFD1901305], Yunnan Fundamental Research Projects [202101AT070002], Wangfeng Expert Primary-level Workstation, Yunnan Province, Intelligent aid to Xinjiang Innovation and Development Talent Plan ("Group Group" aid team) "Environmental functional materials Development and agricultural applications".

Data availability

The datasets used or analyzed during the current study are available from the corresponding author upon reasonable request.

Declarations

Competing interests

All authors certify that they have no affiliations with or involvement in any organization or entity with any financial interest or non-financial interest in the subject matter or materials discussed in this manuscript.

Author details

[1]Ministry of Agriculture and Rural Affairs, Agro-Environmental Protection Institute, Tianjin 300191, China. [2]Dali, Yunnan, Agro-Ecosystem, National Observation and Research Station, Dali 671004, China. [3]College of Life Sciences, Agricultural University of Hebei, Baoding 071066, China.

Received: 1 April 2025 Revised: 3 September 2025 Accepted: 8 September 2025
Published online: 05 January 2026

References

Adeel M, Bilal M, Rasheed T, Sharma A, Iqbal N (2018) Graphene and graphene oxide: Functionalization and nano-bio-catalytic system for enzyme immobilization and biotechnological perspective. Int J Biol Macromol 120:1430–1440. https://doi.org/10.1016/j.ijbiomac.2018.09.144

Aldhahri M, Almulaiky Q, El-Shishtawy M, Al-Shawafi M, Salah N, Alshahrie A, Alzahrani H (2021) Ultra-thin 2D CuO nanosheet for HRP immobilization supported by encapsulation in a polymer matrix: characterization and dye degradation. Catal Lett 151:232–246. https://doi.org/10.1007/s10562-020-03289-7

Almulaiky Q, El-Shishtawy M, Aldhahri M, Mohamed A, Afifi M, Abdulaal H, Mahyoub A (2019) Amidrazone modified acrylic fabric activated with cyanuric chloride: a novel and efficient support for horseradish peroxidase immobilization and phenol removal. Int J Biol Macromol 140:949–958. https://doi.org/10.1016/j.ijbiomac.2019.08.179

Alshawafi M, Aldhahri M, Almulaiky Q, Salah N, Moselhy S, Ibrahim H, El-Shishtawy M, Mohamed A (2018) Immobilization of horseradish peroxidase on PMMA nanofibers incorporated with nanodiamond. Artif Cell Nanomed Biotechnol 46:973–981. https://doi.org/10.1080/21691401.2018.1522321

Bao L, Liu Y, Ding Y, Shang J, Wei Y, Tan Y, Zi F (2022) Interactions between phenolic acids and microorganisms in rhizospheric soil from continuous cropping of *Panax notoginseng*. Front Microbiol 13:791603. https://doi.org/10.3389/fmicb.2022.791603

Besharati Vineh M, Saboury A, Poostchi A, Rashidi M, Parivar K (2018) Stability and activity improvement of horseradish peroxidase by covalent immobilization on functionalized reduced graphene oxide and biodegradation of high phenol concentration. Int J Biol Macromol 106:1314–1322. https://doi.org/10.1016/j.ijbiomac.2017.08.133

Bhardwaj P, Kaur N, Selvaraj M, Ghramh A, Al-Shehri M, Singh G, Arya K, Bhatt K, Ghotekar S, Mani R, Chang W, Ravindran B, Awasthi K (2022) Laccase-assisted degradation of emerging recalcitrant compounds – a review.

Bioresour Technol 364:128031. https://doi.org/10.1016/j.biortech.2022.128031
Biko V, Viljoen-Bloom M, Zyl H (2020) Microbial lignin peroxidases: applications, production challenges and future perspectives. Enzyme Microb Tech 141:109669. https://doi.org/10.1016/j.enzmictec.2020.109669
Bilal M, Iqbal N (2019) Chemical, physical, and biological coordination: an interplay between materials and enzymes as potential platforms for immobilization. Coord Chem Rev 388:1–23. https://doi.org/10.1016/j.ccr.2019.02.024
Bilal M, Rasheed T, Zhao Y, Iqbal HMN (2019) Agarose-chitosan hydrogel-immobilized horseradish peroxidase with sustainable bio-catalytic and dye degradation properties. Int J Biol Macromol 124:742–749. https://doi.org/10.1016/j.ijbiomac.2018.11.220
Bilal M, Bagheri R, Vilar S, Aramesh N, Eguiluz B, Ferreira R, Ashraf S, Iqbal N (2022) Oxidoreductases as a versatile biocatalytic tool to tackle pollutants for clean environment—a review. J Chem Tech Biotech 97:420–435. https://doi.org/10.1002/jctb.6743
Cao X, Zhang N, Zeng Y, Lan L, Ma N, Wu C (2022) Effects of biochar and trichoderma on bacterial community diversity in continuous cropping soil. Hortic Environ Biote 63:1–12. https://doi.org/10.1007/s13580-021-00373-8
Chen P, Wang Y, Liu Q, Zhang Y, Li X, Li H, Li W (2020a) Phase changes of continuous cropping obstacles in strawberry (*Fragaria* × *ananassa Duch.*) production. Appl Soil Ecol. https://doi.org/10.1016/j.apsoil.2020.103626
Chen Q, Man H, Zhu L, Guo Z, Wang X, Tu J, Jin G, Lou J, Zhang L, Ci L (2020) Enhanced plant antioxidant capacity and biodegradation of phenol by immobilizing peroxidase on amphoteric nitrogen-doped carbon dots. Catal Commun 134:105847. https://doi.org/10.1016/j.catcom.2019.105847
Chen B, Wang X, Gao X, Jiang J, Hu M, Li S, Zhai Q, Jiang Y (2021a) DNA directed immobilization of horseradish peroxidase on phase- transitioned lysozyme modified TiO_2 for efficient degradation of phenol in wastewater. Mater des 201:109463. https://doi.org/10.1016/j.matdes.2021.109463
Chen W, Guo X, Guo Q, Tan X, Wang Z (2021b) Long-term chili monoculture alters environmental variables affecting the dominant microbial community in rhizosphere soil. Front Microbiol 12:681953. https://doi.org/10.3389/fmicb.2021.681953
Chen G, Song R, Wang H, Huang L, Wang L, Lei J (2024) Construction of hierarchical porous MIL-100(Fe) for horseradish peroxidase immobilization and its degradation performance of bisphenol A. J Cleaner Prod 481:144178. https://doi.org/10.1016/j.jclepro.2024.144178
Costa-Silva A, Carvalho F, Souza F, Freitas L, Castro F, Oliveira P (2022) Highly effective Candida rugosa lipase immobilization on renewable carriers: integrated drying and immobilization process to improve enzyme performance. Chem Eng Res des 183:41–55. https://doi.org/10.1016/j.cherd.2022.04.026
Cuprys A, Thomson P, Ouarda Y, Suresh G, Rouissi T, Kaur S, Drogui P, Surampalli Y (2020) Ciprofloxacin removal via sequential electro-oxidation and enzymatic oxidation. J Hazard Mater 389:121890. https://doi.org/10.1016/j.jhazmat.2019.121890
Feng Y, Hu X, Guan Y, Chu Z, Du X, Xie Y, Yang S, Ye S, Zhang L, Ma J, Chen H (2024) Regulatory effects of different biochar on soil properties and microbial community structure in chrysanthemum continuous cropping soil. Agronomy 14:2034. https://doi.org/10.3390/agronomy14092034
Fernandez-Sanroman A, Acevedo-García V, Pazos M, Sanromán A, Rosales E (2020) Removal of sulfamethoxazole and methylparaben using hydrocolloid and fiber industry wastes: comparison with biochar and laccase-biocomposite. J Cleaner Prod 271:122436. https://doi.org/10.1016/j.jclepro.2020.122436
Han G, Chen Q, Zhang S, Li G, Yi X, Feng C, Wang X, Yu C, Lan J (2019) Biochar effects on bacterial community and metabolic pathways in continuously cotton-cropped soil. J Soil Sci Plant Nut 19:249–261. https://doi.org/10.1007/s42729-019-0014-z
Hoinacki K, Polidoro S, Cabrera M, Thue S, Jacques A, Lima C, Bussamara R, Fernandes N (2022) Laccase covalently immobilized on avocado seed biochar: a high-performance biocatalyst for acetaminophen sorption and biotransformation. J Environ Chem Eng 10:107731. https://doi.org/10.1016/j.jece.2022.107731
Imam A, Suman K, Singh R, Vempatapu P, Ray A, Kanaujia K (2021) Application of laccase immobilized rice straw biochar for anthracene degradation. Environ Pollut 268:115827. https://doi.org/10.1016/j.envpol.2020.115827
Ji R, Wu Y, Bian Y, Song Y, Sun Q, Jiang X, Zhang L, Han J, Cheng H (2021) Nitrogen-doped porous biochar derived from marine algae for efficient solid-phase microextraction of chlorobenzenes from aqueous solution. J Hazard Mater 407:124785. https://doi.org/10.1016/j.jhazmat.2020.124785
Jia M, Wang X, Zhu X, Du Y, Zhou P, Wang G, Wang N, Bai Y (2024) Accumulation of coumaric acid is a key factor in tobacco continuous cropping obstacles. Front Plant Sci 15:1477324. https://doi.org/10.3389/fpls.2024.1477324
Jing L, Hu Y, Wang T, Hao P, Sun Z, Zhao X, Yin F, Zhang D, Yang H, Zheng Y, Li X, Liu S, Zhang Z, Zhu H (2025) Bionically mineralized ZIF-67-derived adjustable mesoporous FeCoOx/C efficiently immobilize horseradish peroxidase for chloridazon degradation via Fenton and enzyme synergistic catalysis. Chem Eng J 517:164368. https://doi.org/10.1016/j.cej.2025.164368
Kalsoom U, Khalid N, Ibrahim A, Ashraf S, Bhatti N, Ahsan Z, Zdarta J, Bilal M (2023) Biocatalytic degradation of reactive blue 221 and direct blue 297 dyes by horseradish peroxidase immobilized on iron oxide nanoparticles with improved kinetic and thermodynamic characteristics. Chemosphere 312:137095. https://doi.org/10.1016/j.chemosphere.2022.137095
Kumar A, Park D, Patel S, Kondaveeti S, Otari S, Anwar Z, Kalia C, Singh Y, Kim C, Cho K, Sohn H, Kim R, Kang C, Lee K (2019) SiO_2 microparticles with carbon nanotube-derived mesopores as an efficient support for enzyme immobilization. Chem Eng J 359:1252–1264. https://doi.org/10.1016/j.cej.2018.11.052
Li Y, Chen Y, Li T, Song Y, Wu J, Han J, Wang Y (2024) Preparation of thermosensitive polymer immobilized horseradish peroxidase and its application in catalytic degradation of phenol. Catal Lett 154:5683–5697. https://doi.org/10.1007/s10562-024-04730-x
Liu C, Wang W, Wu R, Liu Y, Lin X, Kan H, Zheng Y (2020) Preparation of acid- and alkali-modified biochar for removal of methylene blue pigment. ACS Omega 5:30906–30922. https://doi.org/10.1021/acsomega.0c03688
Liu X, Xue P, Jia F, Shi K, Gu Y, Ma L, Li R (2021) A novel approach to efficient degradation of indole using co-immobilized horseradish peroxidase-syringaldehyde as biocatalyst. Chemosphere 262:128411. https://doi.org/10.1016/j.chemosphere.2020.128411
Liu J, Kim G, Kim B, Abeysinghe S, Lin W, Baek K (2023) Covalent immobilizing horseradish peroxidase on electrochemically-functionalized biochar for phenol removal. Chemosphere 312:137218. https://doi.org/10.1016/j.chemosphere.2022.137218
Mao T, Chen X, Ding H, Chen X, Jiang X (2020) Pepper growth promotion and fusarium wilt biocontrol by *Trichoderma hamatum* MHT1134. Biocontrol Sci Technol 30:1228–1243. https://doi.org/10.1080/09583157.2020.1803212
Maryskova M, Rysova M, Novotny V, Sevcu A (2019) Polyamide-laccase nanofiber membrane for degradation of endocrine-disrupting bisphenol A, 17α-ethinylestradiol, and triclosan. Polymers 11:1560. https://doi.org/10.3390/polym11101560
Morsi R, Bilal M, Iqbal N, Ashraf S (2020) Laccases and peroxidases: the smart, greener and futuristic biocatalytic tools to mitigate recalcitrant emerging pollutants. Sci Total Environ 714:136572. https://doi.org/10.1016/j.scitotenv.2020.136572
Naghdi M, Taheran M, Brar SK, Kermanshahi-pour A, Verma M, Surampalli RY (2018) Pinewood nanobiochar: a unique carrier for the immobilization of crude laccase by covalent bonding. Int J Biol Macromol 115:563–571. https://doi.org/10.1016/j.ijbiomac.2018.04.105
Ng W, Guo H, Ni J, Zhang Q, Chen Z (2022) Effects of soil–plant-biochar interactions on water retention and slope stability under various rainfall patterns. Landslides 19:1379–1390. https://doi.org/10.1007/s10346-022-01874-y
Petronijević M, Panić S, Savić S, Agbaba J, Molnar Jazić J, Milanović M, Đurišić-Mladenović N (2021) Characterization and application of biochar-immobilized crude horseradish peroxidase for removal of phenol from water. Collolid Surface B 208:112038. https://doi.org/10.1016/j.colsurfb.2021.112038
Rasheed U, Ain U, Ali A, Liu B (2024) One stone two birds: recycling of an agri-waste to synthesize laccase-immobilized hierarchically porous magnetic biochar for efficient degradation of aflatoxin B1 in aqueous solutions and corn oil. Int J Biol Macromol 273:133115. https://doi.org/10.1016/j.ijbiomac.2024.133115
Ren J, Jiang N, Shang K, Lu N, Li J, Wu Y (2019) Synergistic degradation of trans-ferulic acid by water falling film DBD plasma coupled with cobalt

oxyhydroxide: performance and mechanisms. Chem Eng J 372:321–331. https://doi.org/10.1016/j.cej.2019.04.147
Ren J, Yao Z, Wei Q, Wang R, Liu Y, Wang L, Zheng K, Wang S, Guo H, Niu Z, Wang J, Han J, Lü L, Zhen Y, Li J (2023) Degradation of ferulic acid and caffeic acid by dielectric barrier discharge plasma combined with Mn/CoOOH/activated carbon fiber. Sep Purif Technol 306:122691. https://doi.org/10.1016/j.seppur.2022.122691
Shen S, Wang Q, Shu J, Ma L, Chen L, Xu Y (2019) Optimization of horseradish peroxidase catalytic degradation for 2-Methyl-6-Ethylaniline removal using response surface methodology. Water 11:1093. https://doi.org/10.3390/w11051093
Taheran M, Naghdi M, Brar K, Knystautas J, Verma M, Surampalli Y (2017) Degradation of chlortetracycline using immobilized laccase on polyacrylonitrile-biochar composite nanofibrous membrane. Stoten 605–606:315–321. https://doi.org/10.1016/j.scitotenv.2017.06.185
Wang Q, Du D, Lu F, Ma Y, Lyu G, Zhang H, Song L (2019) Characteristics of mitochondrial membrane functions and antioxidant enzyme activities in strawberry roots under exogenous phenolic acid stress. Sci Hortic 248:89–97. https://doi.org/10.1016/j.scienta.2018.12.051
Wang Z, Ren D, Zhang X, Zhang S, Chen W (2022) Adsorption-degradation of malachite green using alkali-modified biochar immobilized laccase under multi-methods. Adv Powder Technol 33:103821. https://doi.org/10.1016/j.apt.2022.103821
Wang Y, Liu K, Zhou Y, Chen Y, Jin C, Hu Y (2023) Integrated analysis of microrna and rna-seq reveals phenolic acid secretion metabolism in continuous cropping of *polygonatum odoratum*. Plants 12:943. https://doi.org/10.3390/plants12040943
Wang W, Wu S, Sui X, Cheng S (2024) Phytoremediation of contaminated sediment combined with biochar: feasibility, challenges and perspectives. J Hazard Mater 465:133135. https://doi.org/10.1016/j.jhazmat.2023.133135
Weber C, Silva E, Cordeiro G, Henn S, Costa B, Santos H, Corbellini A, Ethur M, Hoehne L (2023) Immobilization of commercial horseradish peroxidase in calcium alginate-starch hybrid support and its application in the biodegradation of phenol red dye. Int J Biol Macromol 246:125723. https://doi.org/10.1016/j.ijbiomac.2023.125723
Wu J, He T, Ma X, Li C, Han J, Wang L, Dong H, Zhang R, Wang Y (2023) A novel immobilized horseradish peroxidase platform driven by visible light for the complete mineralization of sulfadiazine in water. Int J Biol Macromol 253:127239. https://doi.org/10.1016/j.ijbiomac.2023.127239
Yang Y, Huang X, Dong M, Chang Z, Yuan H, Huang Y, Liu X, Zhang J, Dai A (2024) Fe0Ni0 bimetal co-immobilized horseradish peroxidase on ZIF-8@HMON for degradation of trichloroacetic acid. Chem Eng J 480:147952. https://doi.org/10.1016/j.cej.2023.147952
Yin Q, Chen Z, He P, Liu W, Zhang W, Cao X (2024) Allelopathic effects of phenolic acid extracts on *Morchella* mushrooms, pathogenic fungus, and soil-dominant fungus uncover the mechanism of morel continuous cropping obstacle. Arch Microbiol 206:55. https://doi.org/10.1007/s00203-023-03790-8
Zdarta J, Meyer S, Jesionowski T, Pinelo M (2018) Developments in support materials for immobilization of oxidoreductases: a comprehensive review. Adv Colloid Interface Sci 258:1–20. https://doi.org/10.1016/j.cis.2018.07.004
Zdarta J, Meyer S, Jesionowski T, Pinelo M (2019) Multi-faceted strategy based on enzyme immobilization with reactant adsorption and membrane technology for biocatalytic removal of pollutants: a critical review. Biotechnol Adv 37:107401. https://doi.org/10.1016/j.biotechadv.2019.05.007
Zeng L, Luo D, Liu L, Huang X, Liu Y, Wei L, Xiao T, Wu Q (2023) Alkali/Fe-modified biochar for Cd-As contamination in water and soil: performance and mechanism. Environ Technol Innov 32:103381. https://doi.org/10.1016/j.eti.2023.103381
Zhang H, Yu Y, Weng X, Sun L, Mao C, Zhang L (2019) Degradation of ferulic acid by the endophytic fungus *Colletotrichum gloeosporioides* TMTM-13 associated with *Ostrya rehderiana* Chun. ACS Omega 4:21000–21004. https://doi.org/10.1021/acsomega.9b02225
Zhao Y, Liu F, Yang M, Qi K, Zada A, Pan J (2024) Removal of bisphenol A (BPA) from aqueous solution by potassium carbonate modified wetland plant biochars. Colloid Surface A 703:135184. https://doi.org/10.1016/j.colsurfa.2024.135184